LA-UR -81-3447

MASTER

LA-UR--81-3447

DE82 004374

Los Alamos National Laboratory is operated by the University of California for the United States Department of Energy under contract

TITLE Experiments on Plastic Deformation At Finite Strains

AUTHOR(S) S. S. Hecker, M. G. Stout, and D. T. Eash

SUBMITTED TO Proceedings of "Plasticity of Metals at Finite Strain: Theory, Experiment and Computation," held at Stanford University, CA June 29, 30, and July 1, 1981.

DISCLAIMER

This report was prepared as an account of work sponsored by an agency of the United States Government. Neither the United States Government nor any agency thereof, nor any of their employees, makes any warranty, express or implied, or assumes any legal liability or responsibility for the accuracy, completeness, or usefulness of any information, apparatus, product, or process disclosed, or represents that its use would not infringe privately owned rights. Reference herein to any specific commercial product, process, or service by trade name, trademark, manufacturer, or otherwise does not necessarily constitute or imply its endorsement, recommendation, or favoring by the United States Government or any agency thereof. The views and opinions of authors expressed herein do not necessarily state or reflect those of the United States Government or any agency thereof.

DISTRIBUTION OF THIS DOCUMENT IS UNLIMITED

By acceptance of this article, the publisher recognizes that the U.S. Government retains a nonexclusive, royalty-free license to publish or reproduce the published form of this contribution, or to allow others to do so, for U.S. Government purposes.
The Los Alamos National Laboratory requests that the publisher identify this article as work performed under the auspices of the U.S. Department of Energy

Los Alamos Los Alamos National Laboratory
Los Alamos, New Mexico 87545

EXPERIMENTS ON PLASTIC DEFORMATION AT FINITE STRAINS

S. S. Hecker, M. G. Stout, and D. T. Eash
Los Alamos National Laboratory

ABSTRACT

The strain hardening behavior of metals at large plastic strains is difficult to assess experimentally. Consequently, many different techniques have been used to study such behavior and no clear experimental picture has evolved. In this paper we review experiments on finite plastic deformation with emphasis on work reported since the comprehensive review of Gil Sevillano, van Houtte, and Aernoudt [1]. We are concerned primarily with the macroscopic strain hardening behavior, but discuss its dependence on crystal structure, purity, alloying, microstructure, stacking fault energy, grain size, and deformation mode.

1. INTRODUCTION

The strain hardening behavior of materials is very important in structural response, metal working processes, and, particularly, in plastic instability problems. In metal working and instability analyses a proper description of strain hardening at large plastic strains is imperative. Unfortunately, such descriptions are typically inferred from uniaxial tensile tests, which are restricted to modest strains (typically <0.5) by plastic instability. Such data are not only inadequate, but often misleading. All other test techniques capable of achieving larger strains suffer from experimental difficulties or questionable interpretation. Although a considerable literature has been accumulated for strain hardening of

metals at strains >0.5, no clear picture exists. Large strain deformation has recently been reviewed in an exhaustive treatise by Gil Sevillano, van Houtte and Aernoudt (GVA) [1]. However, since the completion of this treatise a significant amount of new work, including unpublished work by the current authors, has been conducted. We will review the recent work and place it in perspective with previous studies in an attempt to present a current understanding of strain hardening at large plastic strains.

2. BACKGROUND

A most basic question we will examine is whether metals deformed at sufficiently low temperature reach a steady state at large strains and exhibit a saturation flow stress (zero strain hardening). Some early experiments and more recent theoretical analysis by Kocks [2] suggest that face-centered cubic (fcc) metals and alloys should exhibit saturation. More recent experiments summarized by GVA [1] have demonstrated that saturation is definitely not a universal phenomenon. Mecking and Grinberg [3] point out that although steady state behavior should be expected if the evolution of substructure is controlled only by undisturbed dislocation interactions, there are many potential disturbing influences that may appear at large strains. These include i) grain size effects, ii) deformation bands, iii) surface effects, iv) stress-induced transformations (twinning or martensite), v) changing deformation mode, vi) deformational instabilities such as shear bands, vii) texture development, and viii) second-phase particles. Mecking and Grinberg [3] conclude that a unified theoretical model cannot successfully incorporate the influence of all of these factors on strain hardening necessitating experimentation for an

accurate assessment of strain hardening behavior.

From a phenomenological point of view, saturation is assumed in Voce's strain hardening law [4,5] and in the Hockett-Sherby modification [6] as shown in Table I. More simple laws commonly used in plastic analyses predict continued hardening. Kocks [2] has provided a theoretical basis for saturation and derived a strain hardening law similar to the form proposed by Voce.

TABLE I

Phenomenological Models:

Holloman (parabolic)	$\sigma = K\varepsilon^n$
Ludwik	$\sigma = \sigma_o + K'\varepsilon^{n'}$
Swift	$\sigma = K_2(\varepsilon + \varepsilon_o)^{n_2}$
Voce	$\sigma = \sigma_s - (\sigma_s - \sigma_o)\exp(-N\varepsilon)$
Modified Voce (Hockett-Sherby)	$\sigma = \sigma_s - (\sigma_s - \sigma_o)\exp(-N'\varepsilon^p)$
Kocks Model	$\Theta = \Theta_o(1 - \frac{\sigma}{\sigma_s})$ where $\Theta = \frac{d\sigma}{d\varepsilon}\Big\vert_{\dot{\varepsilon},\, T}$

TABLE I. Stress-strain relations based on empirical (phenomenological) and theoretical (Kocks) considerations. The Voce and Kocks relations predict saturation.

The evolution of texture and substructure is a topic worthy of study in its own right. It obviously holds the key to an eventual understanding of strain hardening at large strain. A large amount of information exists on texture development. This subject is adequately covered by GVA [1] and will not be discussed in any detail here. In contrast, substructural studies are not common.

Only in the last few years have transmission electron microscopy studies of through-thickness (or edge-on) sections of heavily deformed metals been conducted. Most of this work has been done on copper and copper alloys [7-17]. A clear understanding of microstructural mechanisms has yet to emerge.

3. REVIEW OF EXPERIMENTAL TECHNIQUES

A great barrier to achieving a better understanding of large strain deformation is the difficulty of conducting decisive experiments. Large-strain experiments are plagued by large changes in specimen geometry and a variety of instabilities, which terminate experiments prematurely. Ideally, strain hardening should be calculated directly from a test that can be run continuously (without interruption) on a uniformly loaded specimen. The stress should be calculated directly from the measured loads and the strains measured directly from the deforming specimen. Table II lists a number of direct and indirect tests and describes their limitations.

Uniaxial tension is restricted to small strains by plastic instability (necking). Few metals can stretch more than 50% before necking. Early attempts to remachine specimens to remove the neck have not become popular. With the advent of closed-loop testing machines it has become more popular to use a diametral extensometer at the neck and control the tensile test with diametral strain. Area and triaxiality corrections are then used to reconstruct a uniaxial tensile curve [18,19]. This method involves a number of assumptions and has yet to be proven. Uniaxial compression is limited by barreling and end effects from the platen. To achieve a true uniaxial stress state excellent lubrication and a length/diameter ratio of ~1.6 are required. Large changes in geometry require

Test Technique	Strain Limits	Comments
Direct Tests		
Uniaxial Tension	<0.5	Plastic Instability
	1 to 1.5	Necking Correction
Biaxial Tension		
(Hydraulic Bulge)	<0.8	Plastic Instability
(Tube Testing)	<0.4	Plastic Instability
Compression	<0.7	Barrelling
	3 to 4	Remachining
Torsion		
Thin-walled tubes	<0.2	Buckling
	2 to 5	Very Short Tubes
Round Solid Bars	2 to 5	Limited by Ductility
Indirect Tests		
Wire Drawing + Tension	10	
Strip Drawing + Tension	4	
Rolling + Tension	7	
+ Plane Strain Compression	7	

Table II. Large strain test techniques and their limitations.

remachining, which has been practiced much more extensively in compression than in tension. It obviously requires starting with a very large specimen. We will present some data of interrupted compression tests to strain levels of ~-4.

Biaxial tension experiments on sheet material are able to produce effective strain levels approximately twice those attainable in uniaxial tension. The added stability under biaxial tension has been discussed by a number of authors [20-23]. Hydraulic bulging offers the best experimental technique for stress-strain measurements of sheet specimens. Unfortunately, there is considerable controversy over the potential errors introduced by

small bulge diameters, biaxial extensometers, and varying strain rates during bulging [24,25]. A much more accurate and versatile technique for biaxial tension is the axial loading/internal pressurization of thin-walled tubes. However, geometric instabilities limit the strain levels to values even lower than those attainable in uniaxial tension [26]. Combined axial/torsion loading of thin-walled tubes suffers from torsional buckling in all but very short tubes, in which end effects may influence stress uniformity.

Torsional deformation offers the best hope for large-strain experiments because it is accompanied by very small geometry changes. However, torsion also suffers from several important restrictions. Experimentally, specimens elongate during torsion and care must be exercised not to restrain their length. Torsion of solid rods also produces an inherently non-uniform stress state, varying from zero at the axis to a maximum at the surface. There has been considerable discussion over the years about how to properly convert a measured torque-angle curve to an effective stress-effective strain curve [27-29]. This makes much of the torsional data in the literature inconsistent because of the different methods of analysis employed. Most recently Canova et al. [30] have developed a technique using several specimens of slightly different diameters to establish an accurate stress-strain curve. The torque-angle conversion to stress-strain is simpler for thin-walled tubes, but torsional buckling limits the strain levels attainable. Apparently some large strain tests have been conducted successfully on very short tubes [31] without adverse end effects.

Most of the large-strain information available in the literature was obtained by one of the indirect tests listed in Table II. These tests are conducted by imparting large prestrains in a deformation mode relatively insensitive to plastic instability (such as wire drawing or sheet rolling) and then testing the prestrained material in uniaxial tension to establish its flow stress level. A series of such prestrains and tensile tests can define a stress-strain curve as shown for our rolling + tension experiments on 1100 aluminum in Fig. 1. Because sheet rolling approximates a state of plane strain it is necessary to adjust the rolling prestrain to an effective strain. We used the von Mises effective strain criterion which gives the correction of $\varepsilon_{eff} = 1.155 \times \varepsilon_t$, where ε_t is the thickness strain during rolling. Similar curves can be constructed for wire and strip drawing. For the case of wire drawing the reduction in area equals the effective strain. Although

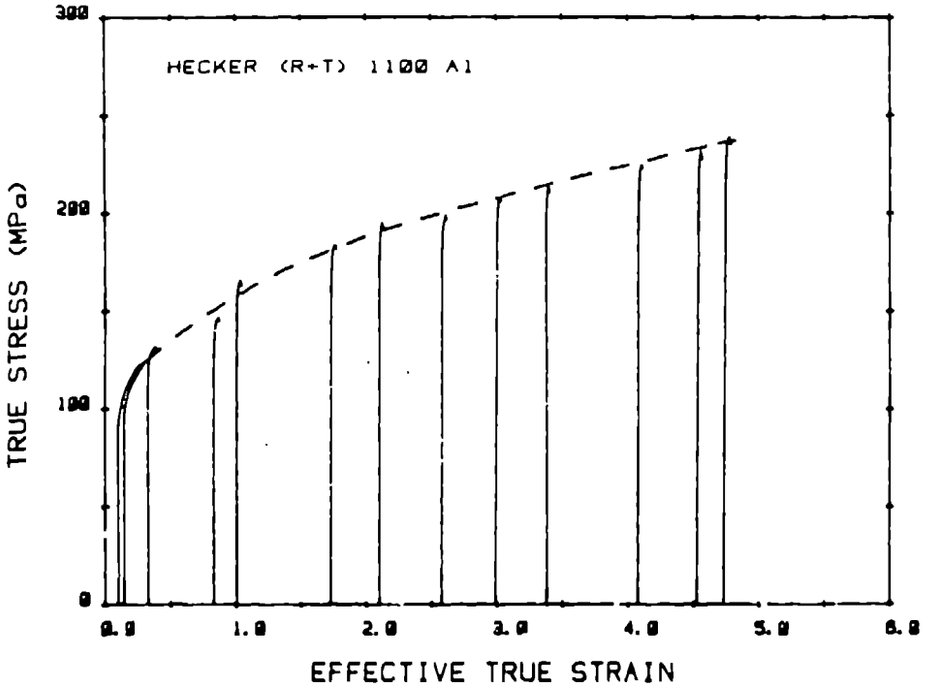

Fig. 1. Construction of a flow stress curve from rolling prestrain followed by uniaxial tension (R+T). The thickness reduction is converted to a von Mises effective strain.

very large strains have been achieved by these techniques (up to 7 in rolling + tension and 10 in wire drawing + tension), these techniques have some obvious drawbacks. The tests are not direct; deformation is incurred under one stress state and the flow stress measured under another. Tests are also interrupted and, in many cases, require remachining of specimens. effective strain criterion must be assumed for proper comparison and in some cases the deformation zone geometry may change during the very large prestrains. The heavily constrained deformation also affects the development of crystallographic texture. Nevertheless, these tests have been used extensively and they provide at least an approximate measure of hardening at large strains.

4. MACROSCOPIC HARDENING BEHAVIOR

4.1. Face-centered Cubic Metals and Alloys

4.1.1. Aluminum and Aluminum Alloys

The hardening behavior of aluminum of different purity levels has been studied extensively. In our laboratory we have deformed commercially-pure aluminum (1100-0) by different techniques. A comparison of flow behavior for tension, compression, and rolling + tension (R+T) is shown in Fig. 2. The compression tests were conducted by Armstrong et al. [33] by repeatedly remachining a large cylinder. The R+T experiments were conducted by the technique described in Section 3. It is quite apparent that hardening for 1100 aluminum continues to very large strains without any sign of saturation. The flow curve for R+T is described accurately by the parabolic expression $\sigma = 155\ \varepsilon^{0.27}$ (MPa). The hardening rate in compression appears somewhat lower at large strains, but these data showed considerable scatter.

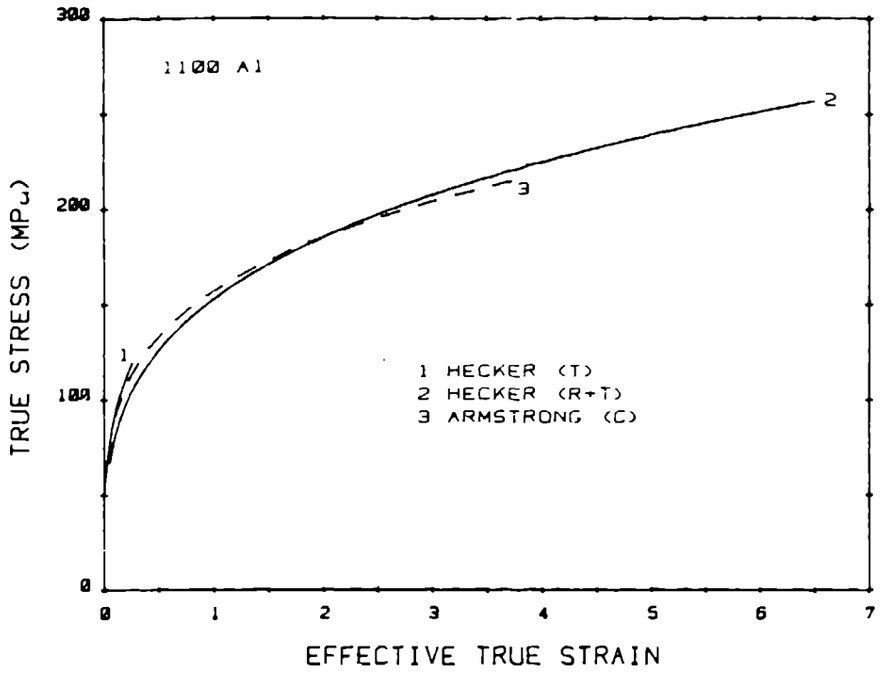

Fig. 2. Comparison of stress-strain curves as determined by tension, rolling + tension, and compression of 1100 aluminum. (References 32 and 33).

LeFevre and coworkers [34,35] measured the flow behavior of a variety of aluminums of different purities using the technique of wire drawing + tension (WD+T). Their results are illutrated in Fig. 3 and compared to our 1100 aluminum data. They show that hardening depends dramatically on purity (or alloying). The high-purity (99.98 Aℓ) aluminum and Aℓ-0.6% Fe alloy show definite signs of saturation. The flow behavior as measured by WD+T and R+T of aluminum alloys with greater amounts of alloying elements are shown in Fig. 4. For Aℓ-4% Cu alloys [14] the effects of heat treatment on hardening are significant. The roles of deformation mode and alloy content and purity are further illustrated in Fig. 5. These results will be discussed in detail below. However, it is quite clear that aluminum of high purity or certain alloy compositions tends towards saturation, regardless of deformation mode.

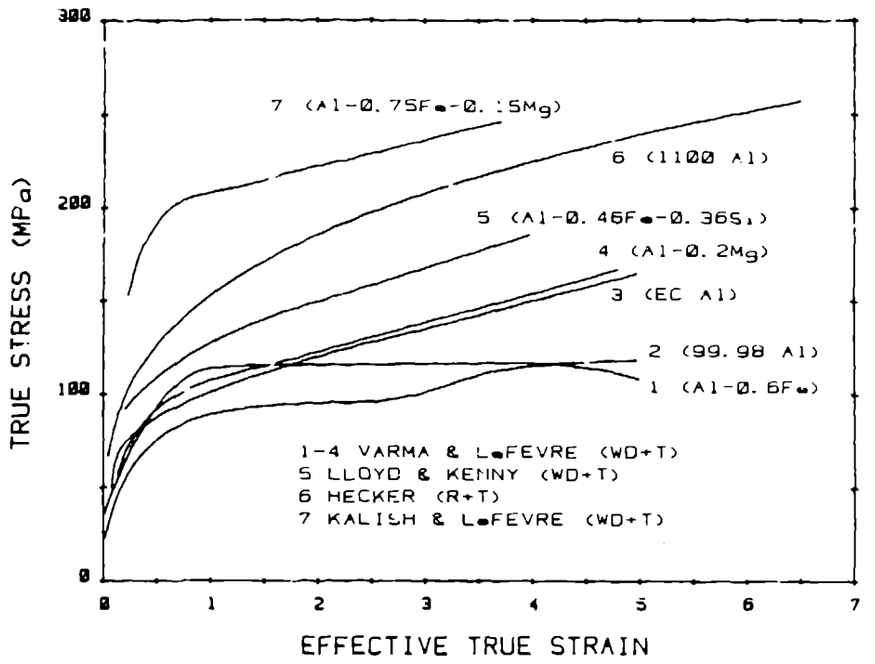

Fig. 3. Stress-strain curves for aluminum of different purities. (R+T) denotes rolling + tension and (WD+T), wire drawing + tension. (References 32, 34-36).

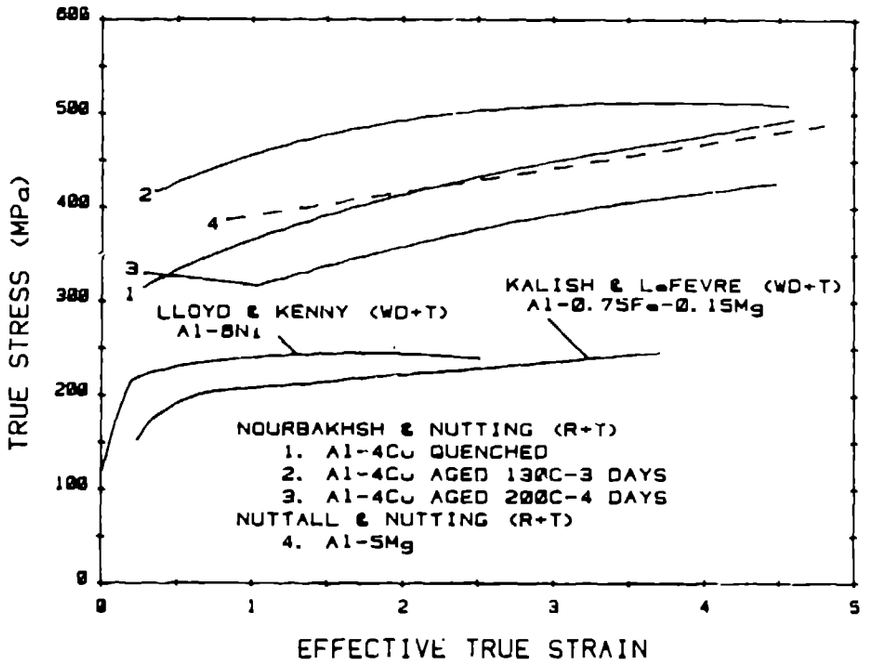

Fig. 4. Stress-strain curves for various aluminum alloys. (References 14, 35, 36, 38).

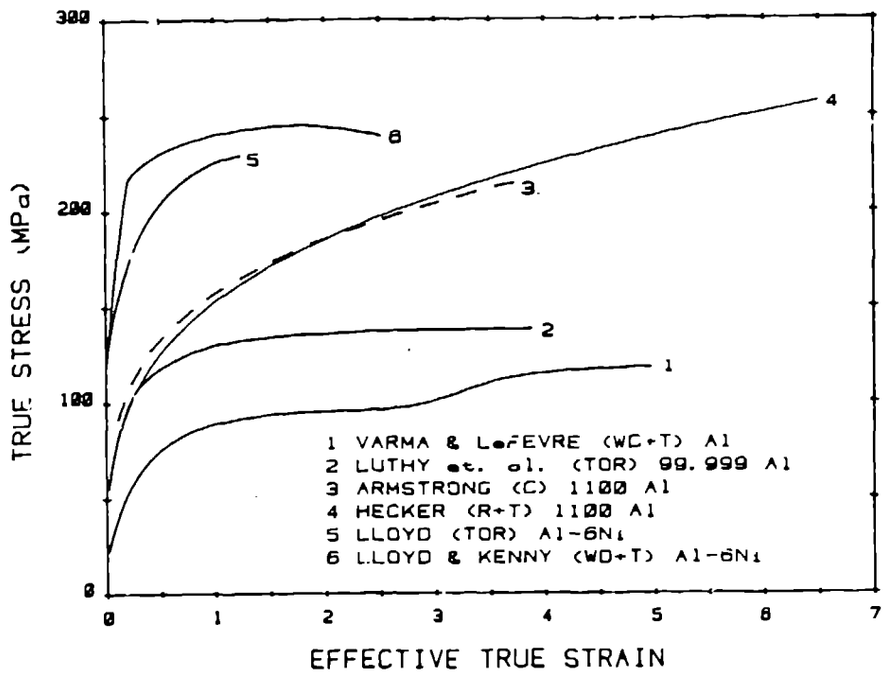

Fig. 5. Comparison of stress-strain curves of aluminum and alloys for different deformation modes. (References 32, 33, 34, 36, 38, 39).

4.1.2. Copper

The large-strain flow behavior of copper for a variety of purities and a number of deformation modes is shown in Fig. 6. Again a tendency towards saturaton for high-purity copper is evident. Only the low-purity ETP copper and phosphorus-deoxidized copper exhibit distinct, continued hardening. The two curves plotted for the data of Cairns et al. [43] represent their and our interpretation of their data. The highest purity (99.999% Cu) copper of Truckner and Mikkola [44] saturates at a very low stress level at a low strain.

4.1.3. Other Face-centered Cubic Metals and Alloys

The flow curves for commercial-purity silver, gold, and nickel are shown in Fig. 7 and compared to commercial purity aluminum and

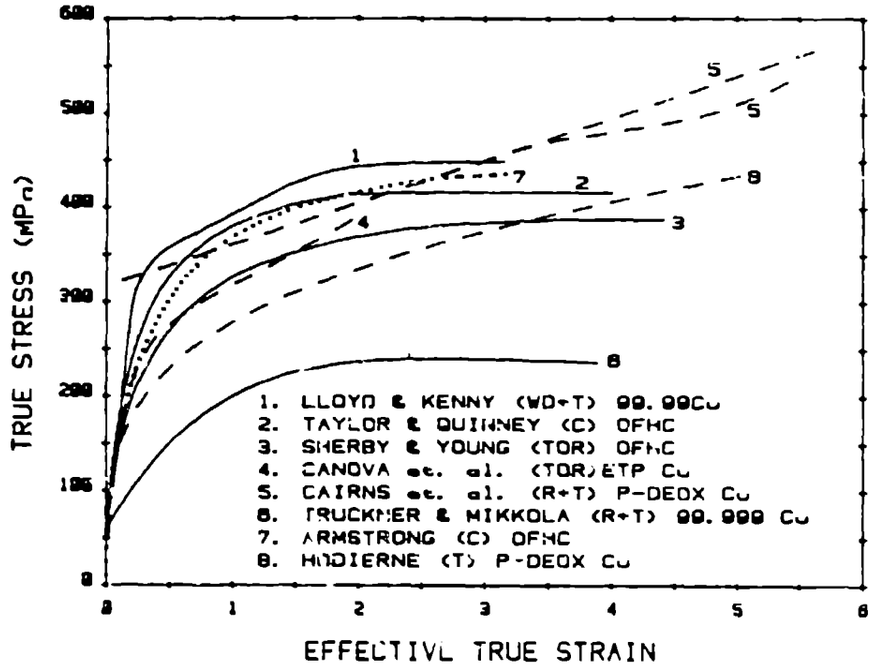

Fig. 6. Stress-strain curves for copper of different purities. (References 30, 31, 40-45).

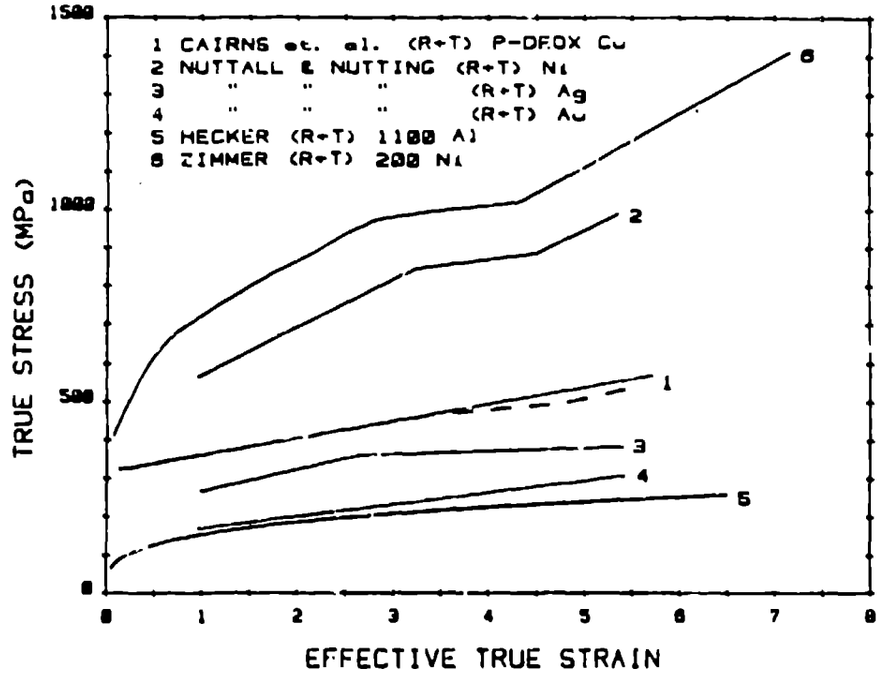

Fig. 7. Stress-strain curves for various fcc metals. (References 32, 37, 43, 46).

copper. All exhibit continuous hardening. The flow curve for silver exhibits a distinct decrease in hardening whereas that for nickel shows a plateau of low hardening rate followed by a very high hardening rate at large strains.

Very few data exist on fcc alloys deformed to strains greater than 2. Hence, the question of strain hardening in fcc alloys remains largely unresolved. Hardening of α brass (typically 70% Cu-30% Zn) appears to continue to large plastic strains, although at a reduced rate from that at smaller strains (Fig. 8). The observation of a much reduced hardening rate in plane-strain tension compared to uniaxial tension (Ghosh [50]) appears valid. The plane-strain tension curve of Ghosh virtually coincides with torsion

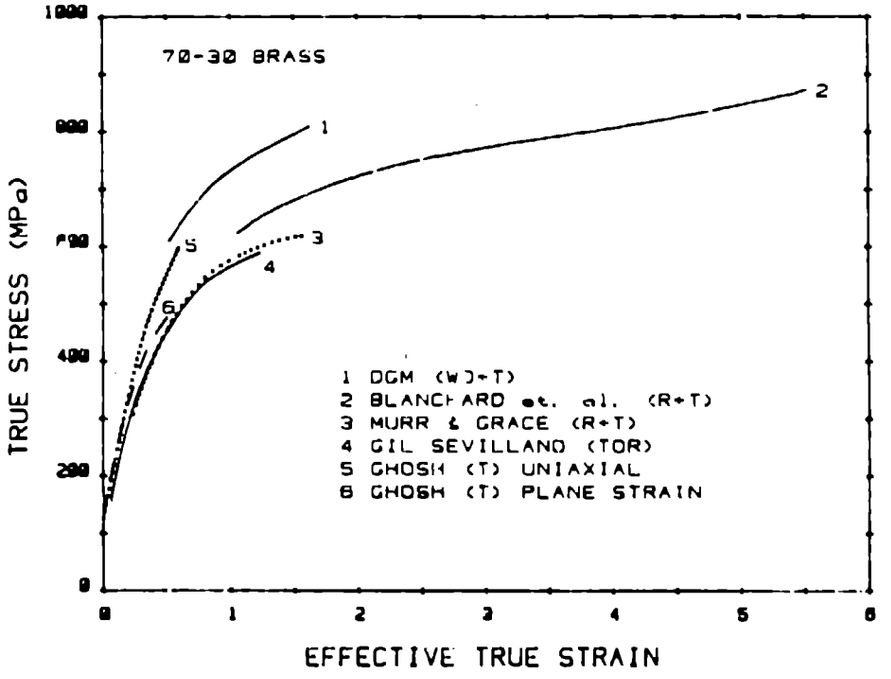

Fig. 8. Stress-strain curves for 70-30 brass for different deformation modes. There appears to be a distinct difference in hardening between axisymmetric (1 and 5) and plane-strain deformation (#2-4 and 6). (References 1, 47-50).

and R+T curves. There is also little evidence for saturation for other copper alloys at large strains (Fig. 9).

Hardening curves for two austenitic stainless steels are shown in Fig. 10. These curves cannot be compared directly because the curve for 20% Cr-26% Ni stainless steel is estimated from hardness measurements. Such extrapolation may give erroneous stress levels and hardening rates. Nevertheless, neither grade of stainless steel exhibits saturation. The initial hardening rate (up to a strain level of 0.5) for grade 302 is very high because this grade is unstable and transforms from fcc γ to bcc α during deformation. The hardening rate remains quite high to the largest strains measured although the transformation to α martensite saturates.

4.2 Body-centered Cubic Metals and Alloys

Most of the available literature on bcc metals and alloys was summarized by GVA [1]. We will present only the highlights here. Perhaps the most dramatic of the bcc results are shown in Fig. 11. Young et al. [53] demonstrated the remarkable difference in hardening behavior of titanium-gettered iron (Fe-0.17% Ti) tested in torsion compared to WD+T. Hardening in torsion (solid rod data converted on the basis of the von Mises criterion) saturates, whereas hardening in WD+T is linear ($\sigma=K\varepsilon$) at large strains. More recent studies by Razavi and Langford [54] confirm the importance of deformation mode. As shown in Fig. 12, the hardening curve for strip drawing followed by tension (SD+T) starts at higher flow stress levels than WD+T, but starts to saturate at a strain similar to the torsion results. These results are similar to those reported for eutectoid steels by Aernoudt and Gil Sevillano [55,56]. GVA [1] reviewed data on other bcc metals such as niobium, tantalum,

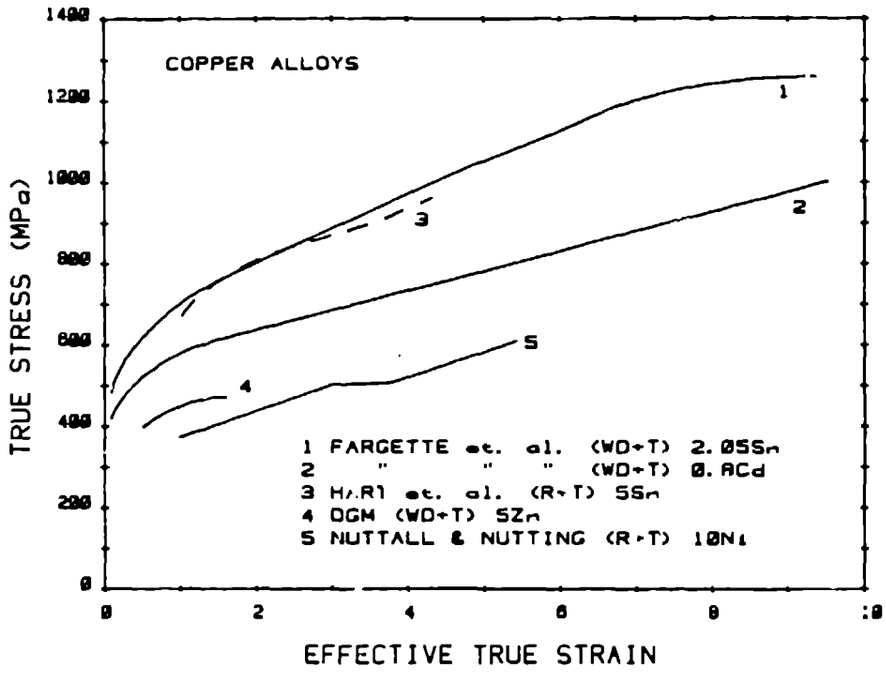

Fig. 9. Stress-strain curves for various copper alloys. (References 37, 47, 51, 52).

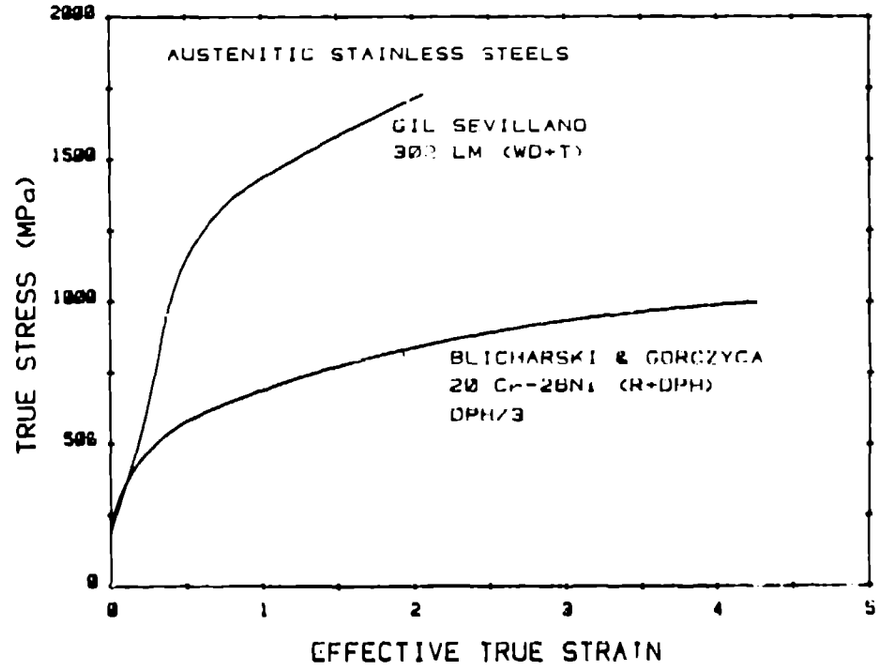

Fig. 10. Stress-strain curves for two austenitic stainless steels. The curve for the 20 Cr-26 Ni steel is estimated from hardness measurements. (References 1 and 10).

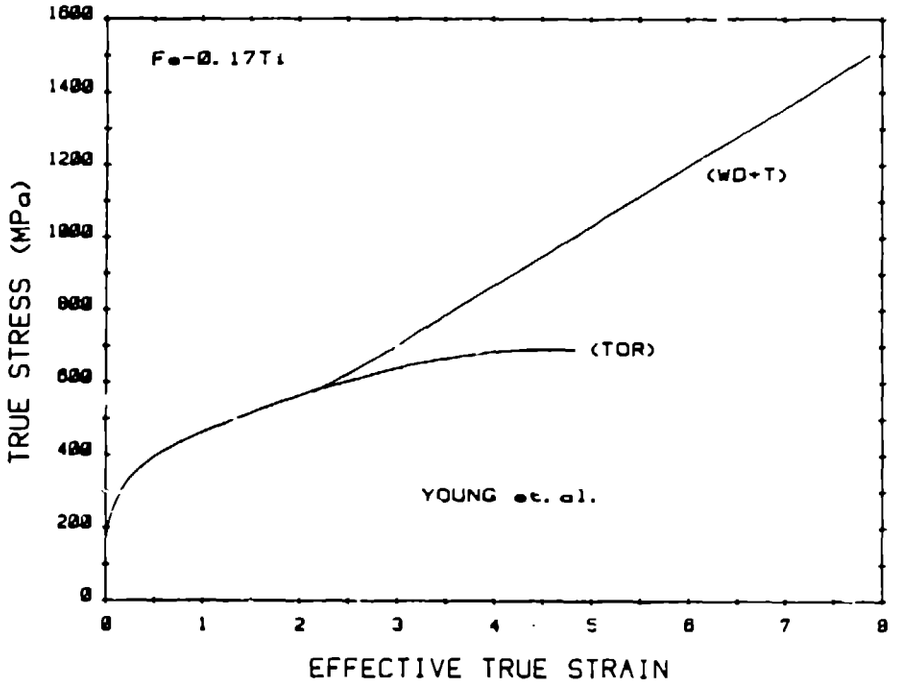

Fig. 11. Comparison of stress-strain curves for Fe-0.17% Ti deformed by torsion and wiredrawing + tension. (Reference 53).

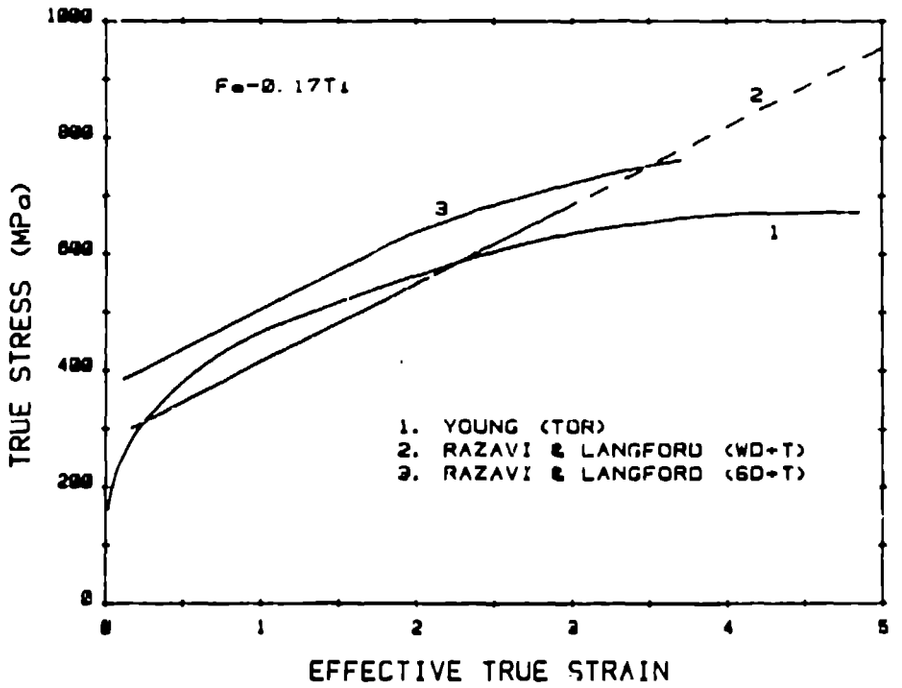

Fig. 12. Comparison of stress-strain curves for Fe-0.17% Ti deformed by torsion, wiredrawing, and strip drawing. The dashed line is a linear extrapolation of Razavi and Langford's data based on other literature values. (References 53, 54).

tungsten, and chromium (the latter two at elevated temperatures). In all cases hardening in WD+T or R+T persists to large strains, regardless of purity. In most cases hardening at large strains is linear.

The effects of interstitial and substitutional alloying levels are shown in Figs. 13 and 14. Both affect the flow stress level, but not the hardening rate. Large increases in carbon levels in plain-carbon steels (Fig. 15) increase both the flow stress and hardening rates. The hardening rate actually increases with increasing strain (upward inflection in Fig. 15) for largely pearlitic steels. The presence of second-phase particles such as inclusions in some steels can cause a dramatic increase in hardening rate as shown by Aghan and Nutting [15,16] for low-carbon steels with sulfur or lead additions (Fig. 16).

4.3 Hexagonal and Other Crystal Structures

Biswas, Cohen, and Breedis [62] showed that hexagonal close packed (hcp) α titanium hardens linearly at large strains in WD+T. The hardening rate increases substantially with increasing interstitial content. Substitutional elements in the α structure appear to have minor effects. Increased purity (iodide Ti) leads to a lower hardening rate, but not to saturation. Recent experiments by Dlicharski, Nourbakhsh, and Nutting [13] on commercially-pure titanium using rolling followed by hardness measurements demonstrated very low hardening at large strains. This may be a result of differences in deformation mode. Zirconium deformed by R+T, also favors low hardening rates at large strains [61].

Very little information exists on metals with other crystal structures. The data of Hockett and Sherby [6] on compression of

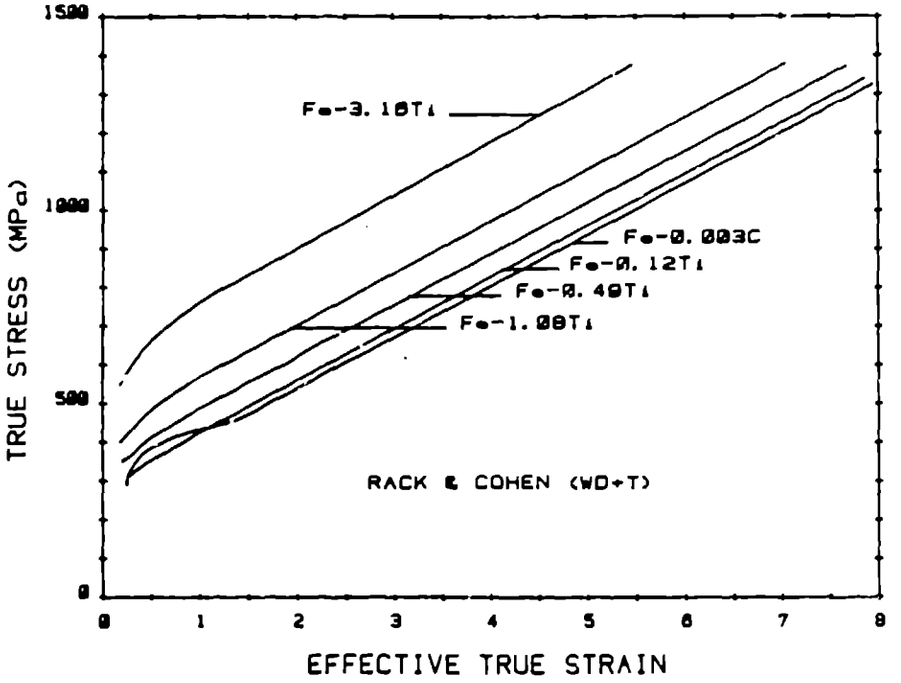

Fig. 13. Stress-strain curves for various Fe-Ti alloys. (Reference 57).

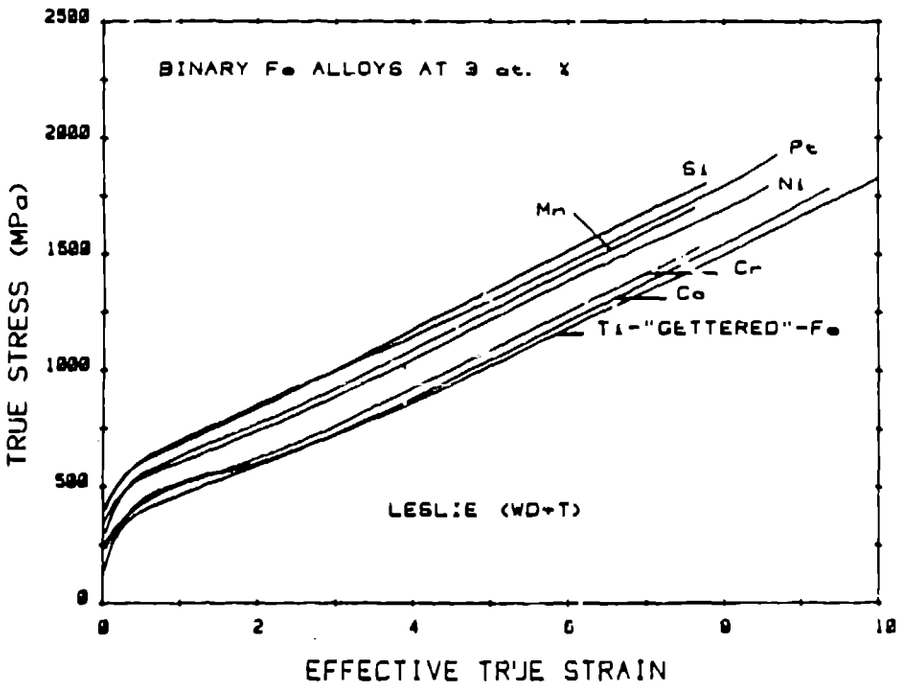

Fig. 14. Stress-strain curves for various iron alloys with different substitutional elements, all present at 3at.%. (Reference 58).

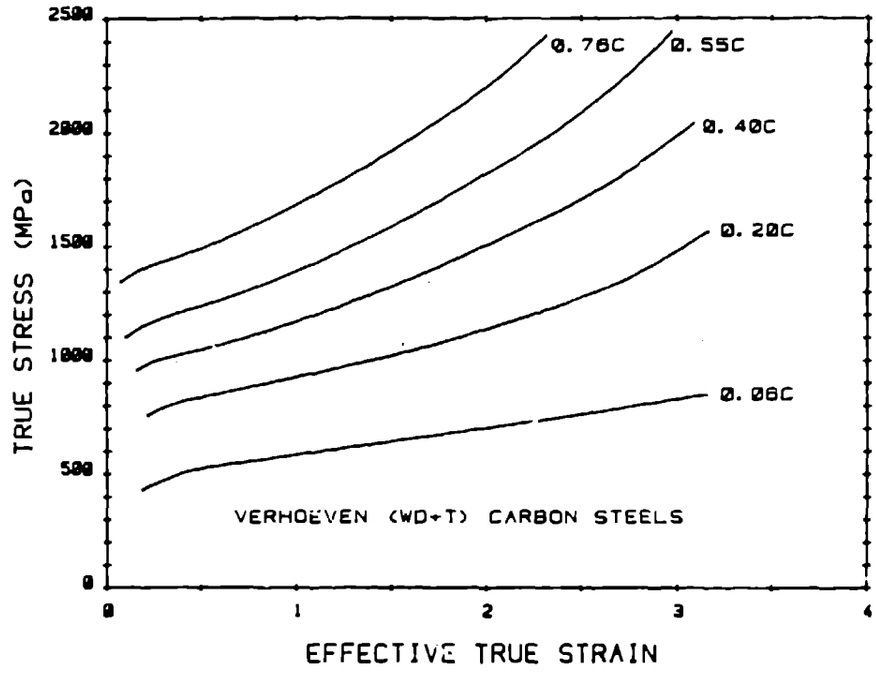

Fig. 15. Stress-strain curves for a series of plain-carbon steels with different carbon levels. (Reference 59).

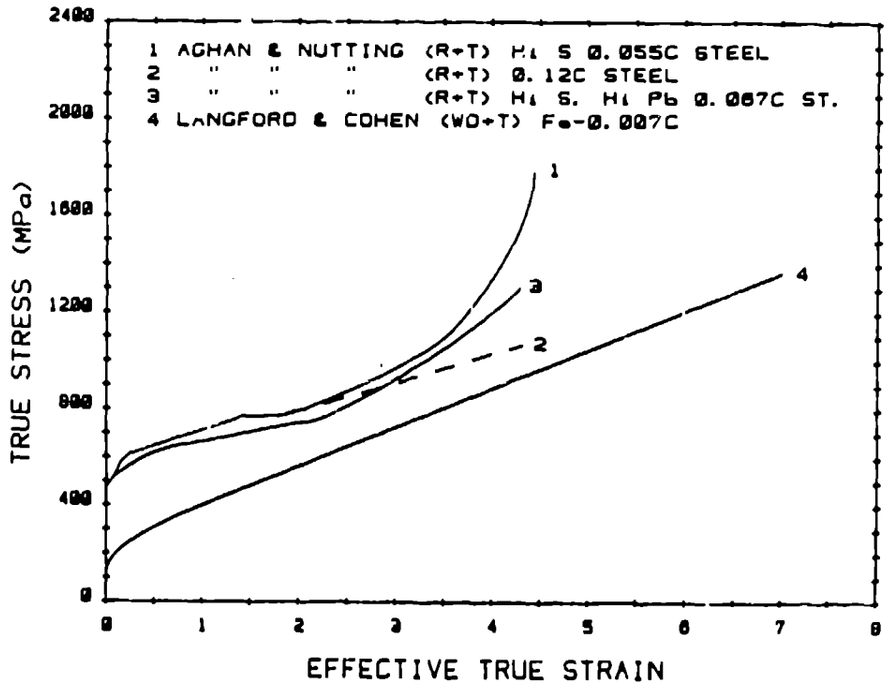

Fig. 16. Stress-strain curves for iron (#4), low-carbon steel (#2), high-sulfur steel (#1), and high-sulfur, leaded steel (#3). (References 15, 16, 60).

orthorhombic α uranium deserves mention because of the enormously high hardening rate. The hardening behavior of α uranium is compared with some typical fcc, bcc, and hcp metals in Fig. 17.

5. DISCUSSION

5.1. Face-centered Cubic Metals and Alloys

5.1.1. Purity

In unalloyed fcc metals purity appears to have an overriding effect on flow stress and hardening rate at low temperatures. We find that regardless of deformation mode, high purity leads to saturation for aluminum and copper. This is illustrated in Figs. 3, 4, and 6. It indicates that dislocation multiplication and annihilation processes control hardening at all strain levels. At large strains the two processes balance each other and a steady state is reached. Other processes such as twinning, shear banding, or texture hardening apparently do not intervene to any significant extent.

In contrast to high-purity metals, commercial-purity fcc metals do not exhibit saturation as demonstrated in Fig. 7. Although the hardening rates for aluminum, gold, and silver are small at large strains, they are definitely positive. The strong role of minor impurities or alloying elements is demonstrated convincingly for aluminum in Fig. 3. No acceptable microstructural explanation exists for the strong role of minor elements. In wire-drawn aluminum Varma and LeFevre [33] showed that there is no simple relationship between minor elements, substructural size, and flow stress. They observed that elements in solution (typically Mg, Si, Zn, and small amounts of Fe) tend to increase dislocation density and decrease cell size for a given amount of reduction. At large

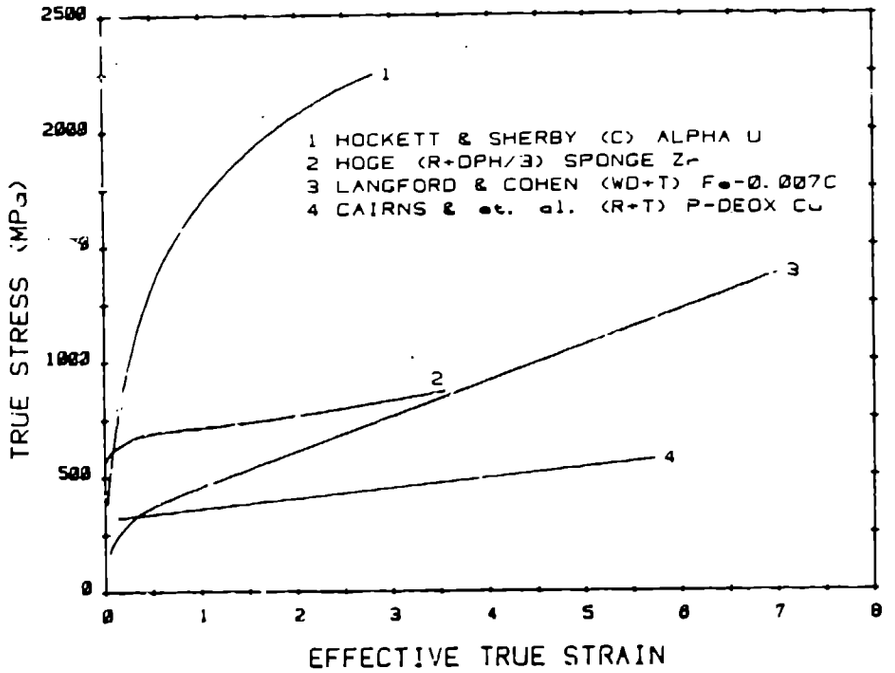

Fig. 17. Comparison of stress-strain curves for metals with different crystal structures. Curve #2 on sponge-Zr is converted from hardness data. (References 6, 43, 60, 61).

strains the degree of recovery and the interrelationship between cell size, cell boundary character, and dislocation density is affected [33].

In rolled aluminum the substructures are not well documented. Typically only the cell dimensions in the sheet surface are examined at large strains and it is not known if the transverse cell dimensions reach a limiting value. We are currently studying the through-thickness cross sections of the 1100 aluminum specimens for which hardening data are shown in Fig. 3.

Moreover, there is considerable doubt that the flow stress is related only to substructural size (or a mean free path). Obstacle strength as manifested by the type of substructural boundaries is also important. Truckner and Mikkola [44] showed that the flow stress in cold-rolled, high-purity copper can be related much more

convincingly to the rms (root mean square) microstrain (which is related to the level of nonuniform strain associated with the dislocation substructure) than to mean free path. The strain softening shown in Fig. 6 corresponds to a decrease in rms microstrain whereas the cell size remains constant.

5.1.2. Alloying and Microstructure

Elements not soluble in the fcc metals can have dramatic effects on hardening. This is demonstrated by the flow curve for Aℓ-0.6% Fe in Fig. 3. The equilibrium solubility of iron in aluminum at room temperature is <0.006 percent. Hence, iron is present as small precipitates of $FeAℓ_3$ or $FeAℓ_6$ [63]. These precipitates tend to nucleate and stabilize cell boundaries during deformation and recovery [34]. The initial hardening is rapid because dislocation density around the particles is very high and the cell size is restricted by the particle dispersion. At strains >1 there is extensive recovery while cell refinement continues, but with no change in dislocation density. As seen in Fig. 3 the flow stress has saturated. At large strains there is evidence of dynamic recrystallization; the cells grow and the flow stress drops [34].

Lloyd and Kenny [36] determined the strain hardening response of an Aℓ-6% Ni alloy. The addition of nickel results in a very fine dispersion of $Aℓ_3Ni$ which restricts the grain size during annealing. This fine dispersion of precipitates causes very rapid initial hardening followed by saturation and work softening. The role of these precipitates at large strains is not clear. They appear to restrict substructural refinement and result in very clean subgrain boundary formation. Figure 5 illustrates that both torsion and wire drawing deformation modes cause saturation.

The alloys in Fig. 3 containing more elements than just iron or nickel (Al-Fe-Mg, Al-Fe-Si, and 1100 Al) also form precipitates. However, these are principally large inclusions (Al-Fe-Si) with large interparticle spacings. These inclusions have little effect on hardening because the substructure is rapidly refined to a size less than the interparticle spacing.

The Al-5% Mg alloy in Fig. 4 shows continuous hardening, much like the Al-0.2% Mg alloy in Fig. 3. The additional magnesium in solution, however, raises the flow stress level by a factor of three. The results of Nourbakhsh and Nutting [14] on Al-4% Cu (Fig. 4) demonstrate the importance of heat treatment and microstructure. Alloys of Al-4% Cu were heat treated to three different microstructures: to produce 1) a supersaturated solid solution of Cu in Al (Curve 1), 2) GP zones (Curve 2), and 3) θ' precipitates (Curve 3). The hardening of the supersaturated solid solution continues at all strain levels, similar to Al-5% Mg. The alloy with GP zones showed initial hardening to a much higher flow stress because of the GP zones contribution. However, at larger strains the GP zones were disrupted and the extra hardening increment lost. Hence, the flow stress actually leveled off and approached that of the supersaturated alloy at large strains. The disruption of GP zones resulted in a decrease in hardening rate. The alloy with θ' precipitates work hardens very rapidly at very low strains to attain a flow stress greater than the supersaturated alloy at a strain of ~ 0.3. However, at this stress level the dislocations cut through the θ' precipitates and the flow stress decreases. Work softening stops at a strain of ~ 1, where most θ' precipitates are cut to

result in a fine dispersion, at which point hardening resumes at a rate similar to the supersaturated alloy.

5.1.3. Stacking Fault Energy

Copper alloys are the only other alloys that have received significant attention. Flow curves for Cu-Sn, Cu-Cd, Cu-Ni, and Cu-Zn alloys in Figs. 8 and 9 indicate that hardening predominates to large strain levels. Several transmission electron microscopy studies of copper and copper alloys [8,9,11,12] indicate that the large strain deformation of medium and low stacking fault energy (SFE) materials is very complicated. In cold-rolled copper microbands (local regions of inhomogeneous deformation of unknown origin) appear below 20% strain, multiply and rotate , and give way to macro shear bands at 90%. In the lower SFE alloys, microbands are followed by profuse twinning and extensive shear banding. Although shear banding is often associated with zero work hardening, the stress-strain curves of Figs. 8 and 9 indicate otherwise. The role of microstructural deformation mechanisms on the hardening response of low SFE materials is not understood and presents a challenging area of study.

Ghosh [50] and Wagoner [64] have demonstrated that for 70-30 brass strain hardening in uniaxial tension is considerably greater than in plane-strain tension at strain levels >0.2. Their test techniques limit the strain levels to <0.6. Figure 8 shows that the plane-strain curve of Ghosh is in good agreement with the rolling + tension curve [49] and torsion curve [1]. We speculate that at large strains, plane-strain favors more extensive twinning and shear banding which may lead to a lower hardening rate. The universality of this hypothesis for all low SFE materials needs to be determined.

One final comment on the role of SFE on hardening. It is well established that SFE is very important in controlling strain hardening at small strains (in the range of a tensile test). Low SFE leads to planar slip and high strain hardening. This is indicated in Fig. 18 by n-values as determined from uniaxial tensile tests ($\varepsilon<0.5$). However, hardening at very large strains ($\varepsilon\sim5$) as expressed by $\Theta=(d\sigma/d\varepsilon)$ shows no simple correspondence with SFE. In fact, for Ag, Au, Cu, and Ni, there appears to be an inverse relationship compared with the small strain case. Moreover, as pointed out above, the hardening rates may decrease to zero for high purity metals. A much better understanding of substructural evolution and its effect on strain hardening at large strains is required. Additionally, the development of crystallographic texture for different deformation modes and its influence on hardening must be considered. GVA [1] present an extensive review. Much progress has been made with crystal plasticity models. However, a clear predictive capability based on crystal structure, stacking fault energy, and temperature still does not exist.

5.1.4. Grain Size

The influence of grain size remains much stronger at large strains than expected. This is illustrated in Fig. 19 for Lloyd's Aℓ-6% Ni alloy [38]. Similar, but more limited information, exists on 70-30 brass and Cu-Si-Mn alloys [1]. One expects the dislocation substructure (cells and subgrains) to govern the flow stress after an initial strain regime where grain size is controlling. The above data suggest that the grain size has a lasting effect on the evolution of substructure. The precise role of grain boundaries at large strains is not well understood because they become obscured

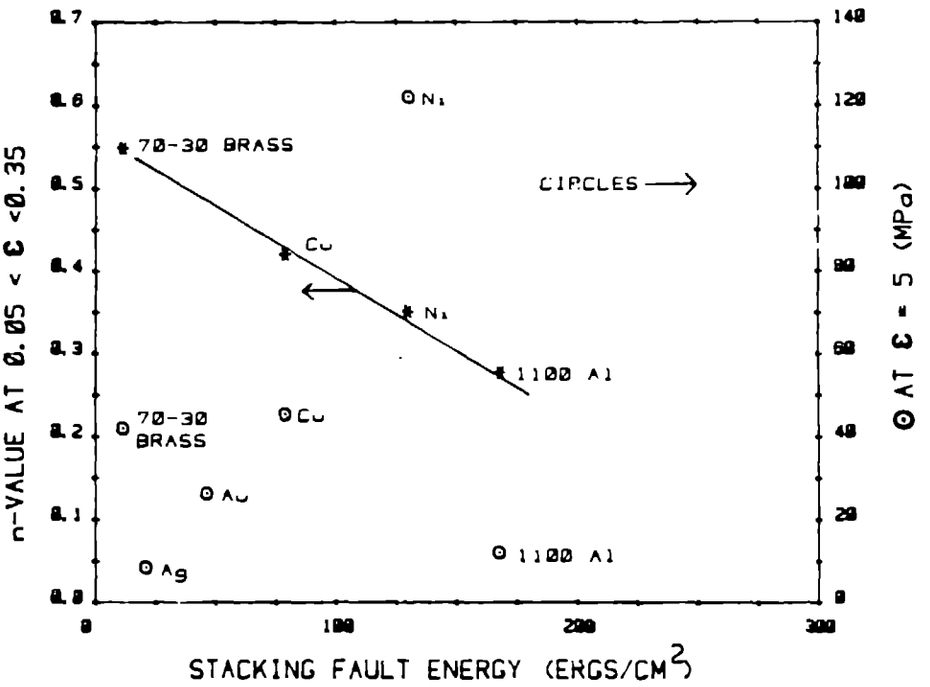

Fig. 18. Comparison of strain hardening at small and large strains. The symbols * refer to n-values as determined from $\sigma=k\varepsilon^n$ at strains between 0.05 and 0.35. The open circles refer to the hardening rate $\Theta=d\sigma/d\varepsilon$ at a strain of 5.

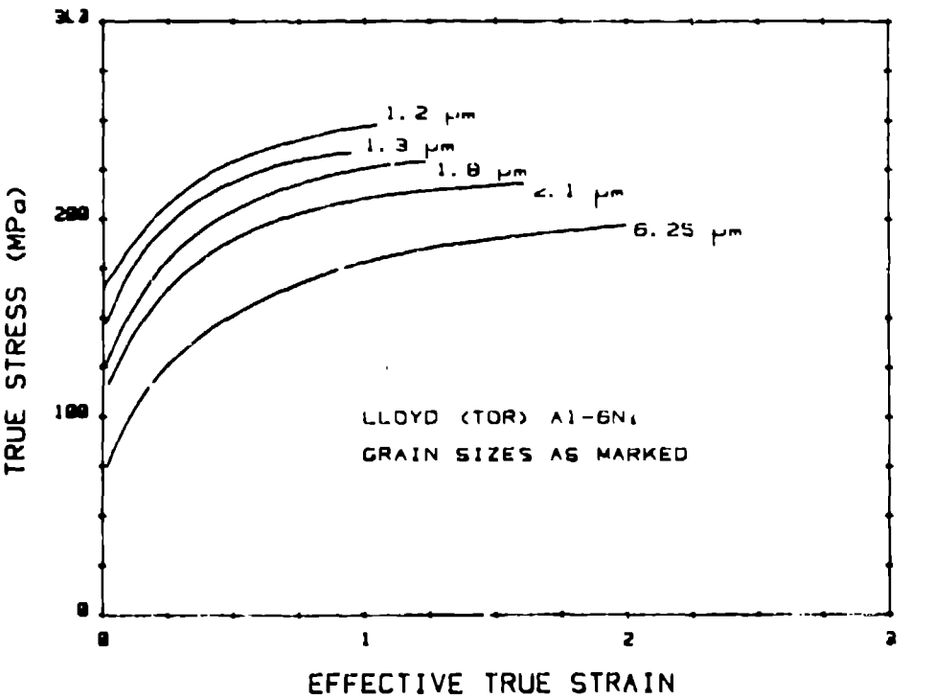

Fig. 19. Stress-strain curves of Al-6% Ni at different grain sizes as marked. (Reference 38).

for transmission microscopy observations at strains >1. It is quite conceivable, however, that grain boundaries play a dominant role in hardening at very small and very large strains as pictured schematically in Fig. 20. At moderate strain levels the formation

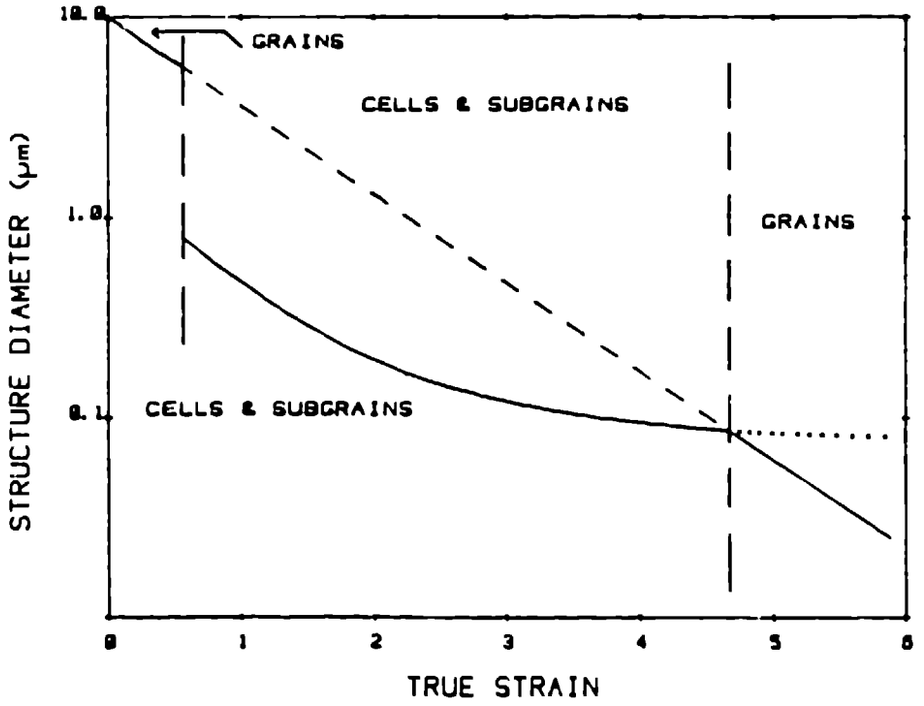

Fig. 20. The potential role of grain and substructure sizes controlling the flow stress. (Reference 1). The dashed diagonal line represents the imposed decrease in transverse grain size by the external shape change due to rolling. The solid curve for cells and subgrains is schematic, but typical for most materials.

of cells and subgrains limit the dislocation mean free path. It is well established experimentally that these substructural dimensions decrease much less rapidly than the imposed grain size change. Hence, it is conceivable that grains become the limiting element again at very large strains (particularly in rolling where the imposed shape change on the through-thickness grain dimension is very rapid). The behavior of nickel in Fig. 7 may represent such a case. To date, no one has presented convincing microscopic evidence

for such a transition. In addition to effects on substructure, it is also conceivable that grain size has an important effect on texture development [65].

5.1.5. Temperature and Strain Rate

The limited amount of information that exists for the effects of temperature and strain rate on strain hardening at large strains is summarized by GVA [1]. The data indicate a continuation of small-strain behavior. Elevated temperature leads to more complete dynamic recovery and saturation [66]. Increased strain rate results in more rapid strain hardening [67]. Although we compare hardening of different materials at room temperature in this paper, it must be recognized that comparison at the same homologous temperature is most appropriate. Unfortunately few systematic studies of large strain deformation over a wide range of temperature have been made.

5.1.6. Deformation Mode

For medium and high SFE materials (copper and above) there is no clear evidence that deformation mode has a significant influence on strain hardening at large strains. There is insufficient data to support Canova et al.'s [30] observations of lower strain hardening in torsion compared to axisymmetric deformation for fcc metals. For fcc alloys with SFE less than copper there is little information about the effect of deformation mode. The data for brass shown in Fig. 8 suggest lower strain hardening in plane-strain tension than in axisymmetric tension. For brass Sundberg et al. [see Ref. 1] showed that rolling followed by tension produced continuous hardening, whereas rolling followed by plane-strain compression produced saturation. It appears that a plane-strain stress state in low SFE materials favors micro and macro-shear banding with a

concomitant reduction in strain hardening. Some definitive experiments are needed to gain a complete understanding.

5.2. Body-centered Cubic Metals and Alloys

Very little information has been generated on bcc metals and alloys since the review of GVA [1]. We will only briefly summarize observations on bcc materials. Figure 13 shows some classical results on high linear hardening obtained in wire drawing plus tension of bcc alloys [57]. Rack, Langford, and Cohen [57,60,68] have demonstrated that this behavior is typical for iron and iron alloys. The strain hardening rate appears to be insensitive to alloying with interstitial or substitutional solids [57,58]. Young, Anderson and Sherby [53] showed that hardening in torsion saturates as demonstrated in Fig. 11. Razavi and Langford [54] recently showed that strip drawing is intermediate between torsion and wire drawing (Fig. 12). Aghan and Nutting [15] demonstrated that low carbon steel exhibits linear hardening during rolling as shown in Fig. 16.

Obviously, unlike the fcc metals, the bcc metals are very sensitive to deformation mode. The explanation for this behavior is still being contested. Several investigators have attributed the difference to texture development. Gil Sevillano and Aernoudt [55,56] claim that most deformation modes lead to hardening and that torsion represents the unusual case. They maintain that because of the texture developed in torsion the slip distance remains unchan at moderate strains and at large strains dynamic recovery actually increases the slip distance. Razavi and Langford [54] relate the continued hardening during wire drawing to redundant strain (curling of grains) necessary to maintain grain continuity. In strip drawing

and torsion, deformation may be accommodated by cooperative rearrangements such as shear banding, leading to a lower hardening rate. Razavi and Langford [54] suggest that the decline in hardening in strip-drawn iron is a result of achieving textural and microstructural stability. Young, Anderson, and Sherby [53,69] explain the difference in hardening between wire drawing and torsion on the basis of substructure. In wire drawing the cells and subgrains continue to be refined and the perfection of the walls increases, whereas in torsion their size saturates. They were able to correlate the flow stress in both cases with the subgrain size and, hence, suggest that texture plays only a secondary role. However, substructural development may well depend on textural evolution and, hence, texture development may still hold the key to the dramatic differences in response between fcc and bcc metals and alloys to different modes of deformation.

The response of multiphase materials to large deformation was also reviewed by GVA [1]. The work of Embury and Fisher [70] and Langford [68] on pearlite is particularly well known. Here we only want to add the recent results of Aghan and Nutting on high-sulfur and lead-bearing steels rolled at room temperature. The flow curves shown in Fig. 16 show a dramatic increase at very large strains. In the case of the high-sulfur steel the MnS inclusions are more plastic than the matrix and, at large strains, a fiber reinforcing effect increases the flow stress above that of plain-carbon steel. In the lead-bearing steel, lead causes the MnS particles to fragment and less reinforcing effect is realized. We use these examples to demonstrate the important role that second-phase particles can play at large strains without having much influence at small strains.

Very little information exists about the effects of temperature and strain rate on bcc materials.

5.3. Other Materials

Only a few studies have been conducted on non-cubic metals and alloys. Biswas, Cohen, and Breedis [62] demonstrated that wire-drawn titanium and titanium alloys (hexagonal close-packed crystal structures) exhibit linear hardening at large strains and found that interstitial elements have a large effect on the hardening rate, whereas substitutional elements have only a minor effect. Blicharski, Nourbakhsh, and Nutting [13] rolled commercial-purity titanium to strains of ~3. Hardness measurements showed rapid hardening to a strain of 1, followed by a low hardening rate (less than most fcc and bcc metals). The accompanying substructural evolution is complicated. Twinning at small strains is followed by slip and then by shear banding with increased deformation. Hoge [61] demonstrated that purity is very important in zirconium, with high purity favoring saturation. Hockett and Sherby [6] reported compression testing result on orthorhombic α uranium. The hardening rate is much higher than any other material. The flow curve for α uranium is compared with those of some fcc, bcc, and hcp metals in Fig. 17.

6. SUMMARY

It is apparent from this review that hardening, not saturation, is the common behavior at large strains. The continuous hardening observed in most materials indicates that the evolution of substructure is not controlled simply by undisturbed dislocation interactions. Other disturbing influences such as texture development, shear bands, and second-phase particles play a major role. Saturation is favored in high-purity fcc metals or in all fcc

metals at sufficiently high temperatures where dynamic recovery is most important and other factors are minimal. In such cases deformation mode appears to have little influence on the question of saturation versus hardening.

In low SFE fcc alloys and in bcc metals and alloys, deformation mode appears important. In low SFE fcc alloys there is some evidence that plane-strain deformation modes favor low hardening and saturation. This may be related to their strong tendency to deform by shear banding. Body-centered cubic metals and alloys exhibit saturation only in torsion. Hardening in plane-strain is intermediate between torsion and axisymmetric deformation. Texture development plays an important role in the hardening behavior of bcc materials.

We attempted to correlate hardening with temperature, crystal structure, and SFE. Figure 21 shows the normalized hardening rate at strains >3 as a function of homologous temperature. Deformation modes were either wire drawing + tension or rolling + tension. We find no clear trend with crystal structure or SFE. There is only a very general trend of increased hardening at lower homologous temperatures.

At present there does not exist a good microstructural basis for deformation at large strains. It represents an area of great challenge and opportunity. The recent work of Dillamore and coworkers [72-75] on texture development and shear banding and the analytical work of Kocks and Chandra [76,77] should prove very stimulating. An understanding of substructural evolution and how the substructure helps to accommodate deformation and control the flow stress is still required.

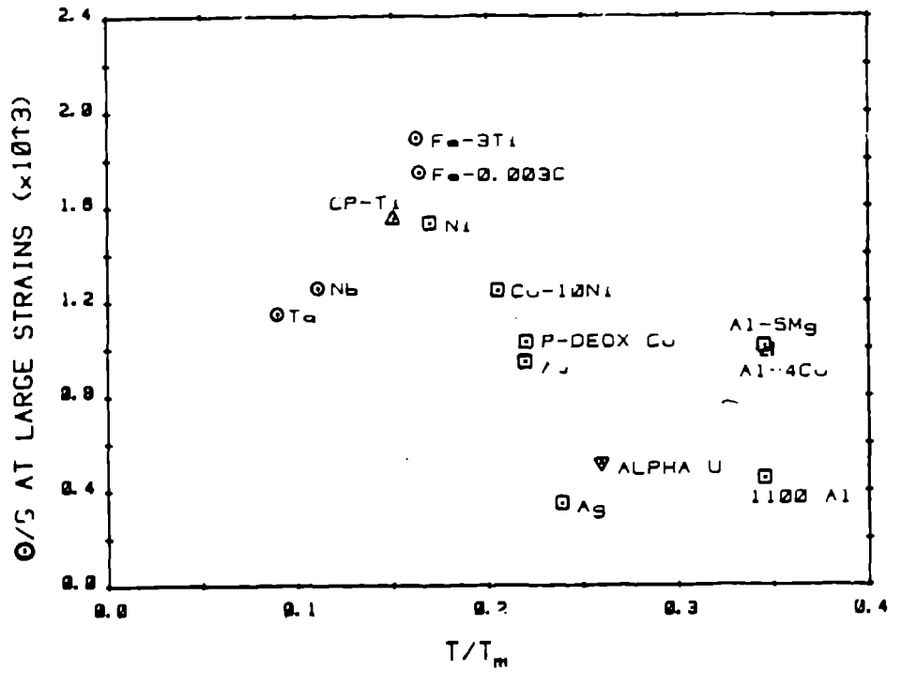

Fig. 21. Normalized hardening rate ($\Theta = d\sigma/d\varepsilon$ normalized by the shear modulus) versus homologous temperature. Hardening rates were taken at large strains from the data compiled in this paper. The hardening rate on Nb is from Ref. 71 and Ta from unpublished work by Gypen and Deruyttere reference in [1]. The symbols represent different crystal structures. Circles represent bcc, squares fcc, up-triangles hcp, and down triangles orthorhombic.

7. ACKNOWLEDGEMENTS

This work was sponsored by the Division of Materials Science, Office of Basic Energy Sciences, US Department of Energy.

8. REFERENCES

1. Gil Sevillano, J., van Houtte, P. and Aernoudt, E., Large Strain Work Hardening and Textures, Progress in Materials Science, 25, pp. 69-412, 1980.

2. Kocks, U. F., Laws for Work-Hardening and Low-Temperature Creep, Journal of Engineering Materials and Technology, Trans. ASME, 98, pp. 76-85, 1976.

3. Mecking, H. and Grinberg, A., Discussion on the Development of a Stage of Steady-State Flow at Large Strains, in Proceedings of 5th International Conference on Strength of Metals and Alloys, ed. Haasen, P., Gerold, V. and Kostorz, G., Pergamon Press, pp. 289-294, 1980.

4. Voce, E., The Relationship between Stress and Strain for Homogeneous Deformation, Journal of the Institute of Metals, 74, pp. 537-562, 1948.

5. Voce, E., A Practical Strain-Hardening Function, Metallurgia, 51, pp. 219-226, 1955.

6. Hockett, J. F and Sherby, O. D., Large Strain Deformation of Polycrystalline Metals at Low Homologous Temperatures, Journal of the Mechanics and Physics of Solids, 23, pp. 87-98, 1975.

7. Schuh, F. and von Heimendahl, M., Die Ausbildung der Versetzungsstruktur in Aluminum und der Beziehungen zum Verformungsverhalten, Z. Metallkunde., 65, pp. 346-352, 1974.

8. Grewen, J., Noda, T., and Sauer, D., Elektronenmikroskopische Untersuchungen an Scherbandern, Z. Metallkunde.. 68, pp. 260-265, 1977.

9. Wakefield, P. T., Malin, A. S. and Hatherly, M., The Structure and Texture of a Rolled Low Stacking Fault Energy Alloy, Journal of the Australian Institute of Metals, 22, pp. 143-151, 1977.

10. Blicharski, M. and Gorczca, S., Structural Inhomogeneity of Deformed Austenitic Stainless Steel, Metal Science 12, pp. 303-312, 1978.

11. Malin, A. S. and Hatherly, M., Microstructure of Cold-Rolled Copper, Metal Science, 13, pp. 463-472, 1979.

12. Hatherly, M. and Malin, A. S., Deformation of Copper and Low Stacking-Fault Energy, Copper-Base Alloys, Metals Technology, 6, pp. 308-319, 1979.

13. Blicharski, M., Nourbakhsh, S. and Nutting, J., Structure and Properties of Plastically Deformed α-Ti, Metal Science, 13, pp. 516-522, 1979.

14. Nourbakhsh, S. and Nutting, J., The High Strain Deformation of an Aluminum-4% Copper Alloy in the Supersaturated and Aged Conditions, Acta Metallurgica, 28, pp. 357-365, 1980.

15. Aghan, R. L. and Nutting, J., Structure and Properties of Free-Cutting Steels After Deformation to High Strains, Metals Technology, 8, pp. 41-45, 1981.

16. Aghan, R. L. and Nutting, J., Structure and Properties of Low-Carbon Steel After Deformation to High Strains, Metal Science, 14, pp. 233-237, 1980.

17. Wakefield, P. T. and Hatherly, M., Microstructure and Texture of Cold-Rolled Cu-10Zn Brass, Metal Science, 15, pp. 109-115, 1981.

18. Hartley, C. S. and Jenkins, D. A., Tensile Testing at Constant True Strain Rates, Proceedings of 6th International Conference on Experimental Stress Analysis, Munich, W. Germany, pp. 379-383 Sept. 18-22, 1978.

19. Hartley, C. S., Jenkins, D. A. and Lee, J-J., Strain Dependence of Strain-Rate Sensitivity, in Proceedings of 5th International Conference on Strength of Metals and Alloys, ed. Haasen, P., Gerold, V. and Kostorz, G., Pergamon Press, pp. 523-528, 1980.

20. Marciniak, Z. and Kuczynski, K., Limit Strains in the Processes of Stretch-Forming Sheet Metal, International Journal of Mechanical Sciences, 9, pp. 609-620, 1967.

21. Keeler, S. P. and Backofen, W. A., Plastic Instability and Fracture in Sheets Stretched Over Rigid Punches, Transactions of the American Society for Metals, 56, pp. 25-48, 1963.

22. Azrin, M. and Backofen, W. A., The Deformation and Failure of a Biaxially Stretched Sheet, Metallurgical Transactions, 1, pp. 2857-2856, 1970.

23. Ghosh, A. K. and Backofen, W. A., Strain Hardening and Instability in Biaxially Stretched Sheets, Metallurgical Transactions, 4, pp. 1113-1123, 1973.

24. Ranta-Eskola, A. J., Use of the Hydraulic Bulge Test in Biaxial Tensile Testing, International Journal of Mechanical Science, 21, pp. 457-465, 1979.

25. Bell, R., Duncan, J. L. and Wilson, I. H., A Sheet-Bulging Machine with Closed Loop Control, Journal of Strain Analysis, 2, pp. 246-253, 1967.

26. Stout, M. G. and Hecker, S. S., Comparison of Plastic Instability in Sheet and Tubular Specimens of 70-30 Brass, presented at Fall TMS/AIME Meeting, Louisville, Ky Oct. 13, 1981. Abstract in Journal of Metals, 33, p. 21, 1981.

27. Nadai, A., Theory of Flow and Fracture, 2nd edition, McGraw Hill Book Company Inc., 1, p. 349, 1950

28. Eichinger, A., Handbuck der Werkstoffprufung, ASTM, 57, pp. 1259, 1957.

29. Fields, D. S. Jr. and Backofen, W. A., Determination of Strain-Hardening Characteristics by Torsion Testing, Proceedings, ASTM, 57, pp. 1259-1272, 1957.

30. Canova, G. R., Shrivastava, S., Jonas, J. J. and G'Sell, C., The Use of Torsion Testing to Assess Material Formability, Prepared for Presentation at the ASTM Symposium "Formability-2000," Chicago, Ill., 1980.

31. Hodierne, F. A., A Torsion Test for Use in Metalworking Studies, Journal of the Institute of Metals, 91, pp. 267-273, 1963.

32. Hecker, S. S., Rohr, D. L. and Aikin, R. M., Unpublished work, Los Alamos National Laboratory, 1978.

33. Armstrong, P. E., Hockett, J. E. and Sherby, O. D., Large Strain Multidirectional Deformation of 1100 Aluminum at 300 K, Submitted to: Journal of the Mechanics and Physics of Solids, 1981.

34. Varma, S. K. and LeFevre, B. G., Large Wire Drawing Plastic Deformation in Aluminum and Its Dilute Alloys, Metallurgical Transactions A, 11A, pp. 935-942, 1980.

35. Kalish, D. and LeFevre, B. G., Subgrain Strenghthening of Aluminum Conductor Wires, Metallurgical Transactions A, 6A, pp. 1319-1324, 1975.

36. Lloyd, D. J. and Kenny, D., The Structure and Properties of Some Heavily Cold Worked Aluminum Alloys, Pre-Publication paper from Aluminum Company of Canada, Ltd. Research Center, Kingston, Ontario, Canada.

37. Nuttall, J. and Nutting, J., Structure and Properties of Heavily Cold-Worked fcc Metals and Alloys, Metal Science, 12, pp. 430-437, 1978.

38. Lloyd, D. J., Deformation of Fine-Grained Aluminum Alloys, Metal Science, 14, pp. 193-198, 1980.

39. Luthy, H., Miller, A. K. and Sherby, O. D., The Stress and Temperature Dependence of Steady-State Flow at Intermediate Temperatures for Pure Polycrystalline Aluminum, Acta Metallurgica, 28, pp. 169-178, 1980.

40. Lloyd, D. J. and Kenny, D., The Stress-Strain Behavior of Copper Over a Large Strain Range, Scripta Metallurgica, 12, pp. 903-907, 1978.

41. Taylor, G. I. and Quinney, H., Proceedings of the Royal Society of London 1, 143, p. 307, 1934.

42. Sherby, O. D. and Young, C. M., Some Factors Influencing the Strain Rate-Temperature Dependence of the Flow Stress in Polycrystalline Solids, Rate Processes in Plastic Deformation of Materials, ed. Li, J. C. M. and Mukherjee, A. K., American Society for Metals, pp. 497-541, 1975.

43. Cairns, J. H., Clough, J., Dewey, M. A. P. and Nutting, J., The Structure and Mechanical Properties of Heavily Deformed Copper, Journal of the Institute of Metals, 99, pp. [illegible]7, 1971.

44. Truckner, W. G. and Mikkola, D. E., Strengthening of Copper by Dislocation Substructures, Metallurgical Transactions A, 8A, pp. 45-49, 1977.

45. Armstrong, P. E., Unpublished Work, Los Alamos National Laboratory, 1979.

46. Zimmer, W., Hecker, S. S., Murr, L. E. and Rohr, D. L., Unpublished Work, Los Alamos National Laboratory, 1979.

47. DGM, Wire Drawing Commission, Fliesskurven verschiedener Werkstoffe, 1975.

48. Blanchard, P., Whitwham, D. and Herenguel, J., Ecrouissage, Restauration, Recristallisation, p. 41, Presses Universitet de France, Paris, 1963.

49. Murr, L. E. and Grace, F. I., Residual Structure and Mechanical Properties of Alpha Brass and Stainless Steel Following Deformation by Cold Rolling and Explosive Shock Loading, Transactions of the Metallurgical Society of AIME, 245, pp. 2225-2235, 1969.

50. Ghosh, A. K., Plastic Flow Properties in Relation to Localized Necking in Sheets, in Mechanics of Sheet Metal Forming-Material Behavior and Deformation Analysis, ed. Koistinen, D. P. and Wang, N-M., pp. 287-312, Plenum Press, 1978.

51. Fargette, B., Whitwham, D. and Diner, O., Bronzes Conducteurs-Cuivre au Cadmium et a L'etain-Influence sur les Proprietes Mecaniques et Electriques de la Deformation a Froid (≅20°C) et du Recuit, Revue de Metallurgie, 65, pp. 679-690, 1968.

52. Hart, R. R., Wonsiewicz, B. C. and Chin, G. Y., High Strength Copper Alloys by Thermomechanical Treatments, Metallurgical Transactions, 1, pp. 3163-3172, 1970.

53. Young, C. M., Anderson, L. J. and Sherby, O. D., On the Steady State Flow Stress of Iron at Low Temperatures and Large Strains, Metallurgical Transactions, 5, pp. 519-520, 1974.

54. Razavi, A. and Langford, G., Strain Hardening of Iron: Axisymmetric vs. Plane Strain Elongation, in Proceedings of 5th International Conference on Strength of Metals and Alloys, ed. Haasen, P., Gerold, V. and Kostorz, G., Pergamon Press, pp. 831-836, 1980.

55. Aernoudt, E. and Gil Sevillano, J., Influence of the Mode of Deformation on the Hardening of Ferritic and Pearlitic Carbon Steels at Large Strains, Journal of the Iron and Steel Institute, 211, pp. 718-725, 1973.

56. Gil Sevillano, J. and Aernoudt, E., On the Influence of the Mode of Deformation on the Hardening of Iron at Low Temperature and Large Strains, Metallurgical Transactions, 6A, pp. 2163-2164, 1975.

57. Rack, H. J. and Cohen, M., Strain Hardening of Iron-Titanium Alloys at Very Large Strains, Materials Science and Engineering, 6, 320-326, 1970.

58. Leslie, W. C., Iron and Its Dilute Substitutional Solid Solutions, Metallurgical Transactions, 3, pp. 5-26, 1972.

59. Verhoeven, F., N. V. Bekaert Internal Reports 503910/2/66 and 503910/5/66, 1966.

60. Langford, G. and Cohen, M., Strain Hardening of Iron by Severe Plastic Deformation, Transactions of the American Society for Metals, 62, pp. 623-638, 1969.

61. Hoge, H. R., Report WAPD-RM-6, Reproduced in The Metallurgy of Zirconium, eds. Lustman, B. and Kerze, F., McGraw-Hill, p. 264, 1955.

62. Biswas, C., Cohen, M., and Breedis, J. F., Strain Hardening of Titanium by Severe Plastic Deformation, Proceedings of the 3rd International Conference on Strength of Metals and Alloys, 1, pp. 16-20, 1973.

63. Stickels, C. A. and Bush, R. H., Precipitation in the System Aℓ-0.05 Wt. Pct. Fe, Metallurgical Transactions, 2, pp. 2031-2042, 1971.

64. Wagoner, R. H., Anomalous Plastic Behavior of 70/30 Brass Sheet, Presented at 1981 TMS/AIME Meeting, Louisville, Ky, Oct. 12, 1981. Journal of Metals, 33, p. 10, 1981.

65. Riegger, S., Vohringer, O. and Macherauch, E., Metallwissenschaft und Technik, 33, p. 1139, 1979.

66. Grewe, H. G. and Kappler, E., Uber die Ermittlung der Verfestigungskurve durch den Torsionsversuch an zylindrischen Vollstaben und das Verhalter von vielkristallinem Kupfer bei sehr hoher Plastischer Schubverformung, Physica Status Solidi,6, pp. 339-354, 1964.

67. Bailey, J. A. and Singer, A. R. E., Effect of Strain Rate and Temperature on the Resistance to Deformation of Aluminum, Two Aluminum Alloys, and Lead, Journal of the Institute of Metals, 92, pp. 404-408, 1964.

68. Langford, G., A Study of the Deformation of Patented Steel Wire, Metallurgical Transactions, 1, pp. 465-477, 1970.

69. Young, C. M., Anderson, L. J. and Sherby, O. D., Reply to "On the Influence of the Mode of Deformation on the Hardening of Iron at Low Temperature and Large Strain", Metallurgical Transactions A, 6A, pp. 2164-2165, 1975.

70. Embury, J. D. and Fisher, R. M., The Structure and Properties of Drawn Pearlite, Acta Metallurgica, 14, pp. 147-159, 1966.

71. Thompson, S. J. and Flewitt, P. E. J., The Defect Structure and Superconducting Transition of Cold-Worked Niobium. Journal of the Less Common Metals, 40, pp. 269-283, 1975.

72. Dillamore, I. L., Lattice Curvatures Produced by the Heavy Deformation of Polycrystals, Texture of Crystalline Solids, 4, pp. 41-56, 1980.

73. Dillamore, I. L., Roberts, J. G. and Bush, A. C., Occurrence of Shear Bands in Heavily Rolled Cubic Metals, Metal Science, 13, pp. 73-78, 1979.

74. Dillamore, I. L., Microstructural Inhomogeneities Resulting from High Strain Deformations, work at University of Aston, to be published, 1981.

75. Dillamore, I. L., Microstructural Modeling of Shear Bands, work at University of Aston, to be published, 1981.

76. Kocks, U. F. and Chandra, H., Slip Geometry in Partially Constrained Deformation, submitted to Acta Met., 1981.

77. Kocks, U. F. and Canova, G. R., How Many Slip Systems, and Which?, Proceedings of Second Riso, Denmark, 14-18 September 1981.